

Basic Neuroscience

Recording from defined populations of retinal ganglion cells using a high-density CMOS-integrated microelectrode array with real-time switchable electrode selection

Michele Fiscella^{a,*}, Karl Farrow^b, Ian L. Jones^a, David Jäckel^a, Jan Müller^a, Urs Frey^c, Douglas J. Bakkum^a, Péter Hantz^b, Botond Roska^b, Andreas Hierlemann^a

^a Bio Engineering Laboratory, ETH Zurich, Basel, Switzerland

^b Neural Circuits Laboratory, Friedrich Miescher Institute, Basel, Switzerland

^c Riken Quantitative Biology Center, Kobe, Japan

HIGHLIGHTS

- ▶ Selection of defined retinal neurons after large-area extracellular screening.
- ▶ Distinct light patterns produce specific neuronal activity without signal artifacts.
- ▶ High-density electrodes enable precise cell allocation and type assignment.

ARTICLE INFO

Article history:

Received 11 March 2012

Received in revised form 15 August 2012

Accepted 16 August 2012

Keywords:

Extracellular recording

Microelectrode arrays

CMOS

Retina

Spike sorting

Light stimulation

ABSTRACT

In order to understand how retinal circuits encode visual scenes, the neural activity of defined populations of retinal ganglion cells (RGCs) has to be investigated. Here we report on a method for stimulating, detecting, and subsequently targeting defined populations of RGCs. The possibility to select a distinct population of RGCs for extracellular recording enables the design of experiments that can increase our understanding of how these neurons extract precise spatio-temporal features from the visual scene, and how the brain interprets retinal signals. We used light stimulation to elicit a response from physiologically distinct types of RGCs and then utilized the dynamic-configurability capabilities of a microelectronics-based high-density microelectrode array (MEA) to record their synchronous action potentials. The layout characteristics of the MEA made it possible to stimulate and record from multiple, highly overlapping RGCs simultaneously without light-induced artifacts. The high-density of electrodes and the high signal-to-noise ratio of the MEA circuitry allowed for recording of the activity of each RGC on 14 ± 7 electrodes. The spatial features of the electrical activity of each RGC greatly facilitated spike sorting. We were thus able to localize, identify and record from defined RGCs within a region of mouse retina. In addition, we stimulated and recorded from genetically modified RGCs to demonstrate the applicability of optogenetic methods, which introduces an additional feature to target a defined cell type. The developed methodologies can likewise be applied to other neuronal preparations including brain slices or cultured neurons.

© 2012 Elsevier B.V. All rights reserved.

1. Introduction

The retina is a multilayered, light-sensitive sheet of neural tissue that encodes visual stimuli as complex spatio-temporal patterns of action potentials. The final output of the retina is encoded in the ganglion cell layer, in which densely packed neurons, called retinal

ganglion cells (RGCs), generate action potentials that proceed along the optic nerve to higher brain regions (Masland, 2001; Wassle, 2004).

Microelectrode arrays (MEAs) are electrophysiological devices for simultaneously recording the extracellular activity of electrogenic cells at multiple spatial positions (Gross et al., 1995; Jimbo et al., 1998; Rutten, 2002; Stett et al., 2003). MEA technology has been widely applied to record electrical activity in the retina (Meister et al., 1994; Segev et al., 2004; Zeck et al., 2011), to investigate retinal development (Anishchenko et al., 2010; Elstrott et al., 2008), retinal connectivity (Field et al., 2010), visual encoding (Gollisch and Meister, 2008; Pillow et al., 2008; Puchalla et al., 2005;

* Corresponding author at: ETH Zürich, Department of Biosystems Science and Engineering (BSSE), Mattenstrasse 26, 4058 Basel, Switzerland.
Tel.: +41 61 387 32 08.

E-mail address: michele.fiscella@bsse.ethz.ch (M. Fiscella).

Schwartz et al., 2007), to evaluate the efficacy of visual restoration techniques (Bi et al., 2006; Lagali et al., 2008), and for the design of artificial retinal implants (Sekirnjak et al., 2008).

Commercially available MEAs usually comprise up to 256 electrodes and feature up to 300 electrodes per mm² (Gross et al., 1995; Pine, 1980) (www.multichannelsystems.com, www.ayanda-biosys.com, www.plexon.com). This density of electrodes is significantly lower than the density of RGCs in many mammals, including rabbits (Oyster et al., 1987), mice (Jeon et al., 1998) and monkeys (Perry and Cowey, 1985). Furthermore, when using conventional MEA technology, it can be challenging to actively target specific cell types for recording, because the electrodes are in a fixed-configuration block, and only the activity of cells that are in the vicinity of these electrodes can be detected.

Recently, high-density MEAs, fabricated in standard microelectronics or CMOS (Complementary Metal Oxide Semiconductor) technology have emerged (Berdondini et al., 2009; Eversmann et al., 2003; Lambacher et al., 2004) and bear the potential to perform recordings from dense populations of neurons at single-cell resolution.

In order to understand how specific features of the visual scene are encoded by the retina, a first step is to examine the synchronously elicited action potentials of defined populations of RGCs (Ackert et al., 2006; Pillow et al., 2008; Schwartz et al., 2007; Trong and Rieke, 2008). To record the activity of a defined population of RGCs, we capitalized upon the electrode configurability capabilities of a CMOS based high-density MEA (Frey et al., 2009). In contrast to an earlier study on blind retinae (Jones et al., 2011), we here used light stimulation to evoke electrical activity from wild type retinae and selected cells according to their light response, which adds to the complexity of the setup and entails the risk of producing artifacts in the recorded signals (see below).

The accurate characterization of a population of neurons is dependent upon the extracellular recording of action potentials with a high signal-to-noise ratio that can be easily differentiated and sorted (Lewicki, 1998). However, light-induced artifacts can introduce erroneous signals and noise into electrophysiological recordings and disrupt the signal analysis process. Such artifacts may arise from the interaction of photons with the electronic components of the CMOS-based circuitry of the MEA chip. Despite the presence of light-sensitive elements in the CMOS-based circuitry, we demonstrate that it is possible to project a light stimulus directly onto the CMOS-based MEA without generating such artifacts in the recorded signals.

Consequently, the absence of light artifacts and the high signal-to-noise ratio allowed us to characterize densely packed RGCs according to their response to light stimulation.

Furthermore, the real-time switchable electrode selection of the MEA allowed the assignment of electrodes to defined physiological types of RGCs. This made it possible to stimulate and record the action potentials from a defined type of RGCs. Finally, it was possible to perform light stimulation of genetically modified RGCs that can be used as optogenetic tools directly on the CMOS-based MEA.

2. Methods

2.1. Data acquisition system

The CMOS-based MEA features 11,011 platinum electrodes with diameters of 7 μm and electrode center-to-center distances of 18 μm over an area of 2 mm \times 1.75 mm (Frey et al., 2009). The centrally located electrode array is surrounded by the signal amplification (0–80 dB), filtering (high pass: 0.3–100 Hz, low pass: 3.5–14 kHz) and analog-to-digital conversion (8 bit) units (Fig. 1a).

Extracellular action potentials can be recorded at high temporal resolution (20 kHz) and with low noise levels ($\sim 7\text{--}9 \mu\text{V}_{\text{rms}}$, band: 100 Hz–3 kHz, perfusion system operational but without retinal tissue). In the maximum-density recording scenario (3161 electrodes/mm²), each mouse RGC lies in close vicinity to multiple electrodes, which allows for recording single-cell action potentials at different spatial locations (Fig. 1b).

A switch matrix circuitry is located under the electrode array and connects the electrodes to 126 readout channels (Frey et al., 2010). An arbitrary subset of 126 electrodes at any location and desired inter-electrode spacing can be routed to the 126 readout channels that surround the electrode array (Fig. 1c).

To reduce the electrode impedance and to improve the signal-to-noise ratio, a layer of Pt-black has been electrochemically deposited onto the electrodes at a current density of 0.5 nA/ μm^2 in a solution containing 7 mM hexachloroplatinic acid, 0.3 mM lead acetate, and hydrochloric acid with an adjustment of the solution pH to 1.

For the purpose of interfacing with the semiconductor chips, custom-designed printed circuit boards have been used. The recorded data are multiplexed and sent via a single twisted-pair cable to a field-programmable gate array (FPGA) board at a rate of 16 MB/s. The FPGA provides data processing features, such as error detection, digital filtering, event detection, and data reduction/compression. The preprocessed data are then sent to a personal computer for further data processing, visualization and storage.

2.2. Projection and alignment of images with the MEA

The light stimuli were designed using Psychtoolbox (<http://psychtoolbox.org>) within the software application MATLABTM and were projected onto the electrode array by an LED projector with a refreshing rate of 60 Hz (Acer K10). The light stimulus was focused only on the electrode array area of the MEA chip by two camera lenses (Nikkor 60 mm 1:2.8 G ED, Nikon), a mirror (U-MBF3, Olympus) and a 5 \times objective (LMPLFLN5X Olympus) (Fig. 1d). The light projection setup was assembled on an upright microscope (BX51WI, Olympus). The MEA chip was positioned with a joystick-controlled system (20 nm resolution along X and Y axis, Scientifica). A video camera provided a real-time view of the electrode array. This procedure enabled the precise projection of a light stimulus exclusively on the electrode array area.

2.3. Preparation of mouse retina and light induced activity recordings

Wild-type C57BL/6J mice (P30) were obtained from Charles River Laboratories (L'Arbresle Cedex, France). All animal experiments and procedures were approved by the Swiss Veterinary Office. The retina was isolated under dim red light in Ringer's medium (in [mM]: 110 NaCl, 2.5 KCl, 1 CaCl₂, 1.6 MgCl₂, 10 D-glucose, 22 NaHCO₃), continuously bubbled with 5% CO₂/95% O₂. The remaining vitreous was removed to improve the contact of the retinal ganglion cells to the electrodes and, finally, a retina patch was placed ganglion-cell-side-down on the electrode array (Fig. 1e). In order to stably secure the retina directly above the MEA, a permeable membrane (polyester, 10 μm thickness, 0.4 μm pore size) was lightly pressed against the tissue; continuous perfusion with oxygenated Ringer's medium at a flow rate of 2.8 ml/minute and at a temperature of 35 $^{\circ}\text{C}$ was provided to maintain tissue viability. Each isolated section of the retina was light-adapted to a "gray" background (blue LED, 460 \pm 15 nm, intensity $\sim 1.0 \times 10^{13}$ photons cm⁻² s⁻¹; green LED, 525 \pm 23 nm, intensity $\sim 1.67 \times 10^{13}$ photons cm⁻² s⁻¹) for a duration of 30 minutes prior to light stimulation and recording. We recorded from mouse

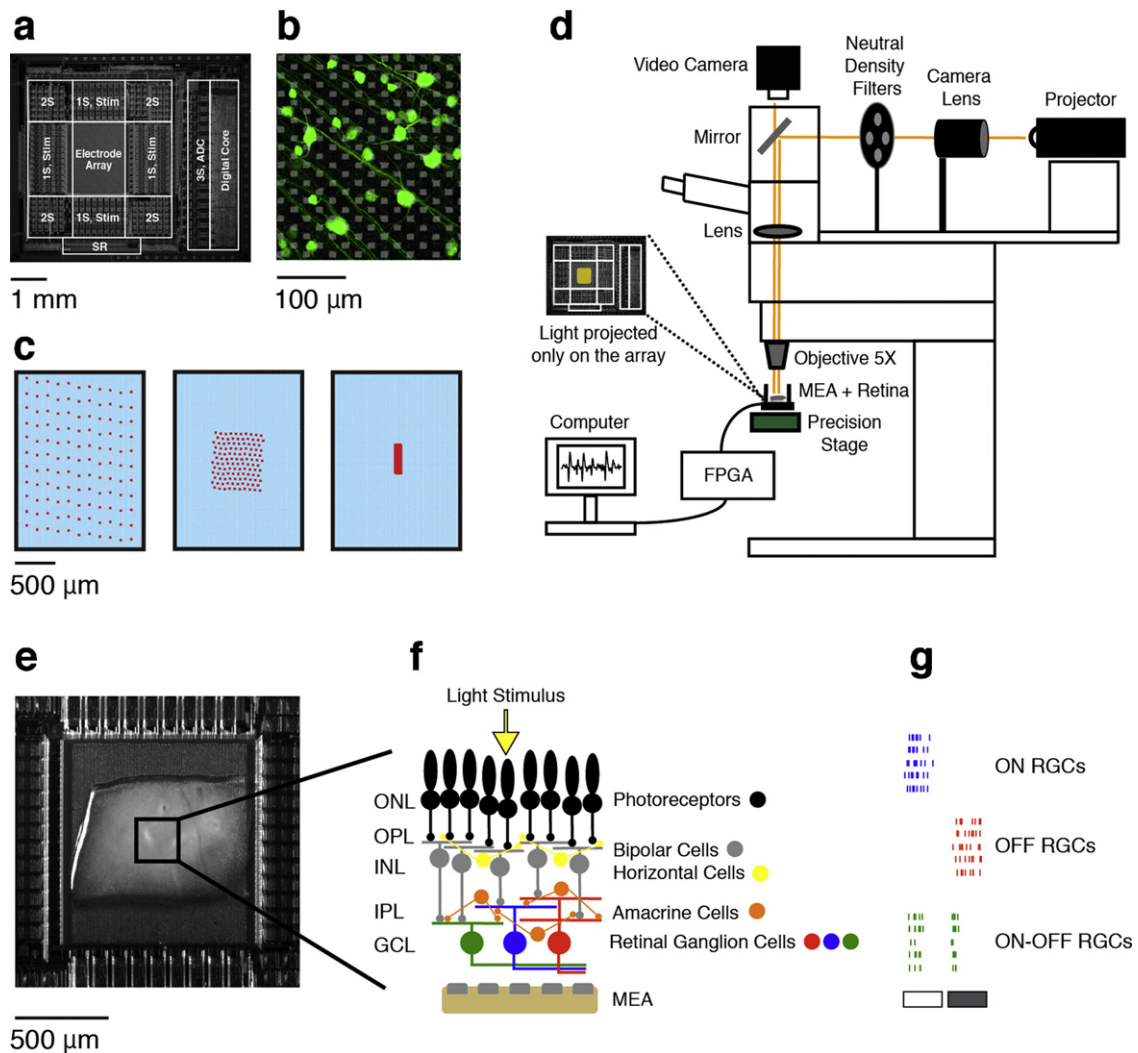


Fig. 1. High-density MEA setup and retinal ganglion cells. (a) Chip micrograph. The electrode array is surrounded by the first-stage amplification and filtering circuitry (1S and 2S) and the stimulation buffers (Stim). Below the array is the shift register (SR) used to program the array, and on the right-hand side are the third amplifier stages, analog-to-digital converters (3S, ADC) and the digital core. (b) Superimposed image of retinal ganglion cells (green) from *Pvalb^{Cre} × Thy1^{Stop-EYFP}* mouse on the electrode array. It can be seen, how each RGC is surrounded constantly by multiple electrodes. This allows the recording of extracellular action potentials simultaneously at multiple sites. (c) Examples of electrode block configurations (~126 electrodes, red squares) that can be dynamically selected from an array of 11,011 electrodes (102 × 108 electrodes) in order to record electrophysiological activity in different regions of the retina. Electrodes can be arbitrarily selected at a desired spacing. Electrode reconfiguration takes ~1 ms. (d) Light projection setup. A light stimulus is generated by a projector and focused only on the electrode array area of the MEA chip by two lenses, one mirror and a microscope objective. The light projection setup is assembled on an upright microscope. The intensity of the light stimulus can be decreased by neutral density filters. A video camera provides a real-time view of the retina on the electrode array. The recorded traces from the MEA chip are sent via a field-programmable gate array (FPGA) board to a computer, where they are stored for further analysis. The light stimulus is centered on the electrode array by a high-precision-movable stage. (e) Mouse retina patch placed ganglion-cell-side-down on the electrode array. (f) Layers of the mammalian retina: ONL, outer nuclear layer; OPL, outer plexiform layer; INL, inner nuclear layer; IPL, inner plexiform layer; GCL, ganglion cell layer. MEA, microelectrode array. A series of computations that will occur through the different retinal layers will convert a light stimulus into action potentials, which are generated by the retinal ganglion cells (indicated by green, blue and red cells) in the GCL. These action potentials can be recorded by the MEA. For more details about cell types and retina layers see *Wassle (2004)*. (g) Three different spike trains belonging to three different types of retinal ganglion cells (ON type, OFF type, ON-OFF type) in response to the same light stimulus (see *Marching Square in Supplementary Material*). The white bar represents a light stimulus brighter than the background light level. The gray bar represents a light stimulus darker than the background light level. Every spike train has a different color and belongs to a different retinal ganglion cell type (Fig. 1f). (For interpretation of the references to color in this figure legend, the reader is referred to the web version of the article.)

retina regions between ~0.7 mm from the edge and ~0.7 mm from the center; the mouse retina features, on average, approximately 2700 retinal ganglion cells/mm² (*Jeon et al., 1998*).

Different sets of light stimuli (see *Light Stimulation in Supplementary Material*) were focused on the photoreceptor layer and elicited action potentials from different types of retinal ganglion cells (Fig. 1f and g).

2.4. Optogenetic stimulation of retinal ganglion cell types

Adeno-associated viruses encoding a channelrhodopsin variant (*Berndt et al., 2009*) (AAV EF1a double floxed ChR2-128S-2A)

were delivered by intravitreal injection into the eyes of the *Pvalb^{Cre}* transgenic mouse (*Yonehara et al., 2011*). A minimum of 14 days incubation time was kept to achieve channelrhodopsin expression in the Cre-expressing RGCs. In order to identify RGCs expressing ChR2 on the MEA, we blocked photoreceptor-mediated light responses in the retina by the application of a drug cocktail containing 10 μM ABP (2-amino-4-phosphonobutyrate, agonist of the mGluR6 receptors of the ON-pathway), 10 μM CPP (3-[(±)-2-carboxypiperazin-4-yl]-propyl-1-phosphonic acid, an NMDA receptor antagonist) and 10 μM NBQX (2,3-dihydroxy-6-nitro-7-sulfamoyl-benzo[f]quinoxaline-2,3-dione, a kainate AMPA antagonist). Light stimulation was performed by a flash of 40 ms,

with an intensity of $\sim 1.6 \times 10^{17}$ photons $\text{cm}^{-2} \text{s}^{-1}$ and a wavelength of 470 ± 20 nm.

During drug application, light-induced action potentials could originate from RGCs expressing Chr2, or from intrinsically photosensitive retinal ganglion cells (ipRGCs) (Berson et al., 2002; Wong et al., 2007). The activity of RGCs expressing Chr2 and the activity ipRGCs could be separated based on the response latency to light stimulation. In control conditions with wild type retinæ (without RGCs expressing Chr2), the probability to find light responses with latencies between 0 and 50 ms was 3.9% (Fig. 7b). In experiments with *Pvalb^{Cre}* transgenic retinæ (with RGCs expressing Chr2), we found that 41% of the total response latencies were less than 50 ms (Fig. 7b).

Therefore, these RGCs in *Pvalb^{Cre}* transgenic retinæ, with latencies less than 50 ms, were treated as Chr2-responding cells.

2.5. Data analysis

Offline Spike Sorting was performed, on data acquired after an experiment, by a principal-component analysis (PCA) – K-means based algorithm (Duda et al., 2001; Lewicki, 1998).

Online Spike Sorting was performed in order to select a specific population of RGCs during an experiment. For this purpose, we used an independent-component-analysis (ICA) based algorithm (Brown et al., 2001; Jackel et al., 2012) (For details, see Spike Sorting in Supplementary Material).

2.6. Imaging of mouse retinal ganglion cells

For imaging of RGCs we used the retina from the mouse line *Pvalb^{Cre} × Thy1^{Stop-EYFP}*. The retina was assessed with a Zeiss LSM 700 confocal microscope, 40× oil immersion lens, NA 1.2, 0.5× digital zoom.

3. Results

3.1. Light induced artifacts in CMOS technology and light evoked retinal activity

An important development was the elimination of noise introduced into the recordings by light-induced artifacts; this enabled us to record the electrogenic activity of RGCs without any interference caused by the light stimulation.

The light artifact phenomenon, which can introduce noise or offset in the electrical signal output, is due to light sensitivity characteristics exhibited by the active circuitry of CMOS-based MEAs. It is caused by photon-induced charges in the electronic components such as diodes or transistors. However, most of the short-wavelength fraction of the incident light will not pass the chip passivation layer stack, which consists of alternating layers of silicon nitride and silicon oxide of a total thickness of 1.6 μm and has been additionally applied on the chip surface to protect the chip components against penetration of liquids and associated chemical and electrochemical corrosion. The oxide-nitride layers show absorption below a wavelength between 500 and 450 nm depending on the nitride/oxide chemical composition, stoichiometry and deposition method (Ding et al., 2009). Additionally the retina patch ($\sim 250 \mu\text{m}$ thick) will absorb a part of the incident light.

Two cases have been considered for the device used here: the first includes light falling only on the sensor, i.e., the electrode array area (Fig. 2a – top row), the second includes light falling also onto the readout circuitry, where the most light sensitive elements are located (Fig. 2a – bottom row).

In the first case, we found that the electrode area and the underlying switch matrix are not sensitive to the light intensities and

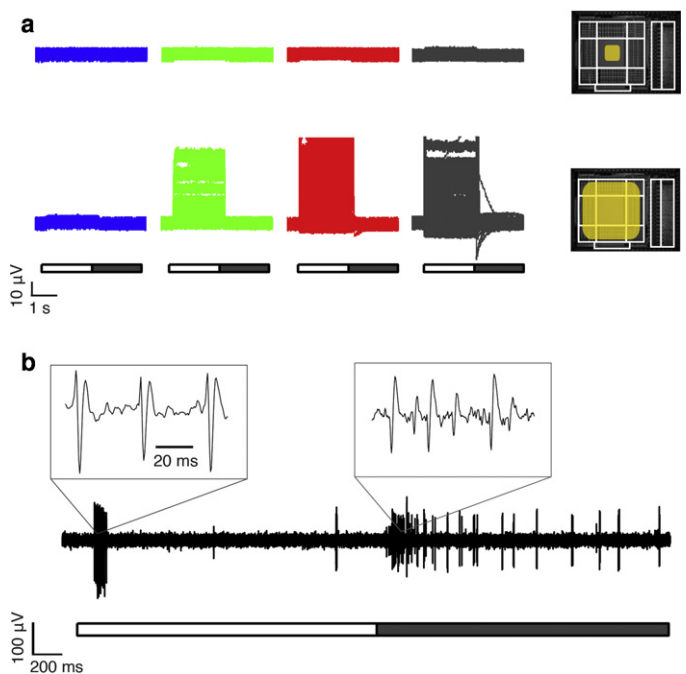


Fig. 2. Light artifact on CMOS circuitry and light response of retinal ganglion cells. (a) Top row: response of 126 recording channels to a light stimulus (represented by yellow-colored square) projected onto the electrode array only. Bottom row: response of 126 recording channels to light projection onto the readout circuitry and onto the electrode array. White bars represent “light on” and gray bars “light off.” Note the absence of artifacts, when light is projected exclusively on the array. The color of the traces corresponds to the following wavelengths and intensities: blue: 460 ± 15 nm; intensity $\sim 2.0 \times 10^{13}$ photons $\text{cm}^{-2} \text{s}^{-1}$; green: 525 ± 23 nm; intensity $\sim 3.3 \times 10^{13}$ photons $\text{cm}^{-2} \text{s}^{-1}$; red: 640 ± 12 nm; intensity $\sim 2.3 \times 10^{13}$ photons $\text{cm}^{-2} \text{s}^{-1}$; gray: intensity $\sim 1.2 \times 10^{14}$ photons $\text{cm}^{-2} \text{s}^{-1}$ (blue, green and red sources active at the same time). (b) An example of ON and OFF light-evoked responses from mouse RGCs, as recorded by the MEA. The white bar indicates the projection of a light stimulus brighter than the background light level (“light on”). The gray bar indicates the projection of a light stimulus darker than the background light level (“light off”). The action potentials as recorded on one electrode are shown. We used the following wavelengths and intensities to elicit light-induced action potentials: blue: 460 ± 15 nm; intensity $\sim 2.0 \times 10^{13}$ photons $\text{cm}^{-2} \text{s}^{-1}$; green: 525 ± 23 nm; intensity $\sim 3.3 \times 10^{13}$ photons $\text{cm}^{-2} \text{s}^{-1}$. (For interpretation of the references to color in this figure legend, the reader is referred to the web version of the article.)

wavelengths used in our retinal experiments (Fig. 2a – top row). In the second case, the surrounding readout circuitry was found to be light-sensitive, and was characterized by a greater sensitivity to longer wavelengths of light (Darmont, 2009) (Fig. 2a – bottom row). The most light sensitive elements in this device are the cross-coupled diodes, used as pseudo-resistors in the feedback of the amplifiers to achieve a very low high-pass filter cut-off frequency (Frey et al., 2010). Thus, when light hits the amplifiers, photo-induced charges cause artifacts in the recorded signal by adding offset and noise in the amplified signal (Fig. 2a – bottom row) and may even saturate the amplifiers or bring the amplified signal out of the range of the analog-to-digital converter.

Finally, to avoid any light-induced artifacts, light was exclusively projected onto the 3.5 mm^2 electrode array area during the experiments. As such, it was possible to record light-evoked action potentials from RGCs in the absence of light-induced artifacts in the recorded signals (Fig. 2b).

3.2. Characterization of mouse extracellular action potentials

To determine the magnitude and spatial spread of signals produced by mouse RGCs, we analyzed approximately 60,000 extracellular light-evoked action potentials from four

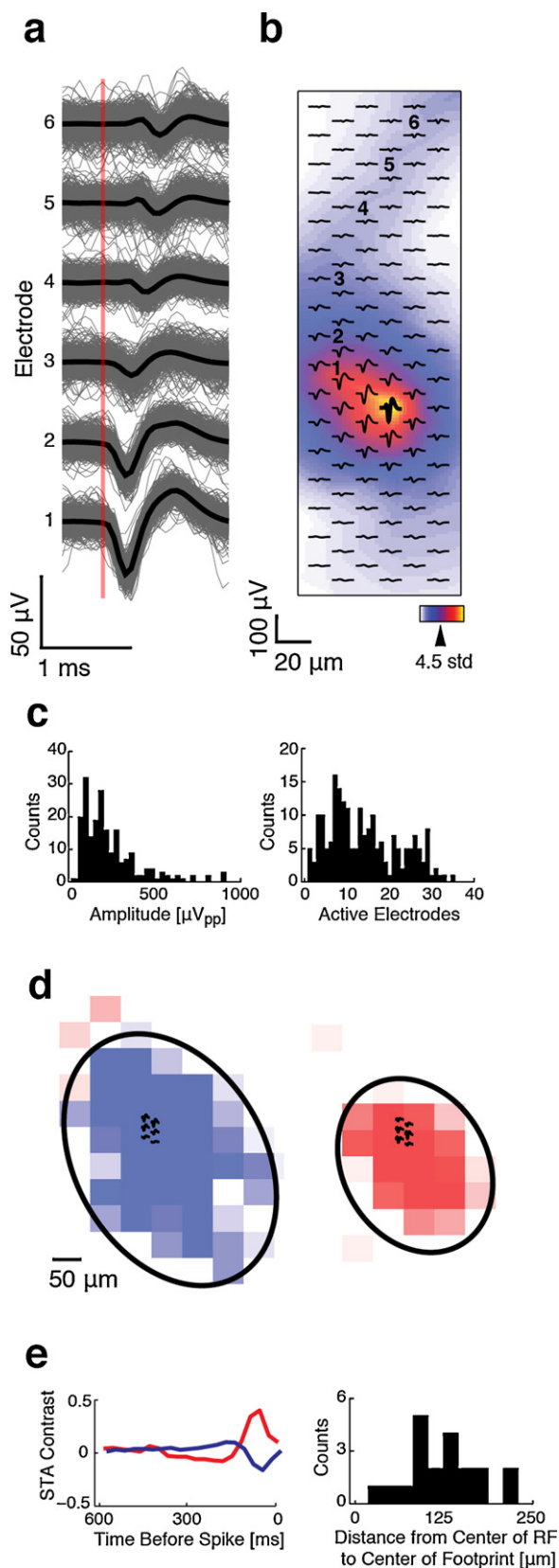


Fig. 3. Characterization of extracellular action potentials from mouse retinal ganglion cells. (a) Superposition of 959 action potentials (gray traces) from six electrodes, indicated in (b). The propagation speed, evident by the staggered timing from the initial depolarization of electrode 1, was calculated to be 0.7 m/s. A biphasic somatic action potential is shown (electrode 1) as well as tri-phasic axonal action potentials (electrode 6). (b) Spatial distribution (footprint) of averaged signals of a single RGC over an area of 0.025 mm². The thick black waveform indicates highest

different retinal preparations using high-density electrode blocks (3161 electrodes/mm²).

On the CMOS-based MEA chip used here, single-cell action potentials were consistently detectable on multiple electrodes, and the propagation of action potentials along axons was observable (Fig. 3a and b).

Among the electrodes used to record the signal generated by any given cellular action potential, the central electrode (the electrode with the highest signal) recorded peak-to-peak amplitudes of $230 \pm 170 \mu\text{V}$ (Fig. 3b and c – left panel). The signal amplitude declined, as one moved away from the central electrode such that on average each action potential was recorded with 14 ± 7 electrodes (Fig. 3c – right panel). This number of electrodes covers an area equivalent to $65 \mu\text{m} \times 65 \mu\text{m}$, and all action potentials recorded within this area had a negative peak exceeding 4.5 standard deviations of the noise level. As expected, the action potential of a single RGC was distributed over a region that is larger than the cell body (Gold et al., 2006), as shown in previous retinal studies (Segev et al., 2004), or in recordings of neurons from other brain regions (Frey et al., 2009). In the mouse retina, the soma diameter of RGCs varies between $10 \mu\text{m}$ and $30 \mu\text{m}$ (Sun et al., 2002) explaining the variability observed in the spatial spread of the footprint. Furthermore, the amplitude and spatial distribution of the action potential are not only influenced by the cell morphology and distance to the recording electrodes, but also by the density of voltage sensitive ion channels and the myelination of the axon (Boiko et al., 2001; Gold et al., 2006).

Finally, the soma of mouse RGCs tends to be located within its dendritic field area (Sun et al., 2002), which approximately corresponds to the receptive fields of the cells (Brown et al., 2000). The receptive field of a RGC is the region of space, in which the presence of a light stimulus will alter or cause the firing of that RGC (Chichilnisky, 2001; Meister et al., 1994). Accordingly, we found that the center of the electrical footprint was located within each cells receptive field and the average distance between the central electrode of a footprint and its receptive field center was $120 \pm 50 \mu\text{m}$ (Fig. 3d and e).

3.3. Separation of retinal ganglion cells action potentials

In order to characterize the light responses of individual mouse RGCs, action potentials must be correctly assigned to the corresponding neurons. As described above, high-density electrode recording techniques enable the visualization of the electrical footprint of each neuron (Fig. 3b). In order to assess, whether the additional spatial information of the action potential improves the accuracy of spike waveform assignment, we used a basic spike sorting algorithm, based on Principal Component Analysis (PCA) and K-means clustering method (Lewicki, 1998) in an off-line procedure.

peak-to-peak amplitude (central electrode). Color code (right corner), yellow-red indicates the region of maximum signal amplitude (active electrodes with action potential negative peak 4.5 standard deviations above the noise level). (c) Left panel: distribution of action potential peak-to-peak amplitudes for 206 RGCs mouse at the electrode with highest signal ($230 \pm 170 \mu\text{V}$). Right panel: distribution of the number of active electrodes for 206 mouse RGCs (14 ± 7 active electrodes). (d) ON and OFF mouse RGC footprints (black action potential waveforms) and their receptive fields. The receptive fields are determined by examining the spike-triggered average (STA) stimulus 60 ms before a spike (Chichilnisky, 2001). These two neurons were recorded on the same subset of electrodes. (e) Left panel: temporal contrast of the STA at the receptive field center. Right panel: distribution of distances between the center of receptive fields and the center of 20 RGCs footprints ($120 \pm 50 \mu\text{m}$). (For interpretation of the references to color in this figure legend, the reader is referred to the web version of the article.)

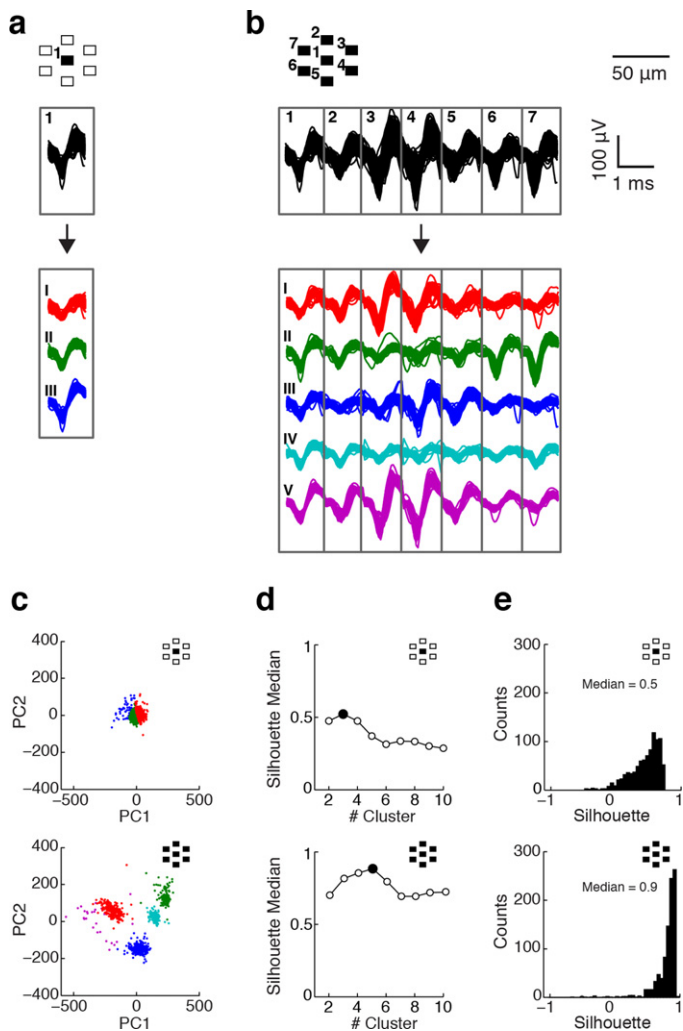


Fig. 4. Spike sorting with high spatial electrode density. (a) 939 action potentials isolated from the central electrode (black square). The surrounding electrodes (white squares) where not used. After spike sorting, action potentials were clustered into three groups (red, green, blue clustered waveforms), representing three putative neurons. The percentages of refractory period violations (0–2 ms) in the inter-spike interval distribution were 7%, 3% and 0%, respectively. (b) 939 action potentials isolated from the central electrode (black square in center) concatenated to synchronously recorded waveforms from six surrounding electrodes. After spike sorting, action potentials were clustered into five groups (red, green, blue, cyan, purple), and none of them had violations in the inter-spike interval distribution. The absence of violations is an indicator of correctness of sorting. (c) Principal component (PC) projection of spike waveforms from (a) (top panel) and (b) (bottom panel). The PC projection is used to cluster the action potential. (d) Medians of silhouette coefficient distributions as function of the number of clusters for waveforms from (a) (top panel) and (b) (bottom panel). The solid black circles indicate the optimal clustering solution with the highest median value (see also Fig. S1). (e) Distribution of silhouette coefficients for clustered waveforms from (a) (top panel) and (b) (bottom panel). The median values correspond to the solid black circles in (d). (For interpretation of the references to color in this figure legend, the reader is referred to the web version of the article.)

We compared the results of separating the spike waveforms, obtained from a single electrode, and those from different combinations of neighboring electrodes. (Fig. 4a and b, Fig. S1).

The quality of spike sorting was assessed by estimating the percentage of refractory period violations (0–2 ms) in the inter-spike interval distributions of the sorted neurons (see [Spike Sorting in Supplementary Material and Fig. S1](#)). The refractory period is the time needed for the membrane of a neuron to come back to its resting state before a new action potential can be fired. This time is typically between 1 and 2 ms and implies that the interval between

two consecutive action potentials cannot be less than ~ 2 ms. Consequently, the presence of inter-spike intervals of less than ~ 2 ms, among the action potentials assigned to a single neuron, indicate an incorrect spike sorting.

In order to determine how many different neurons were in the recorded waveforms, we used the silhouette coefficients (Rousseeuw, 1987). After PCA and K-means clustering, every action potential is represented by a score in the PCA space and it is assigned to a cluster (Fig. 4a–c). For every action potential, assigned to a cluster in the PCA space, a silhouette coefficient can be computed, which measures how similar that point is to points within the same cluster as compared to points in the other clusters. The silhouette coefficients vary between -1 and 1 , which respectively indicate “misclassified” or “well-clustered” data. The clustering solution with the highest median, computed from the distributions of the silhouette coefficients, was chosen as the correct solution (see [Spike Sorting in Supplementary Material and Fig. S1](#)).

In Fig. 4a, spike waveforms, which were isolated from only a single electrode, are shown. The best clustering solution, with the highest median silhouette value, produced three groups (Fig. 4c and d – top panel). Each of the three putative RGCs had refractory period violations of 7%, 3% and 0%, respectively.

In Fig. 4b, the signals simultaneously recorded from the six surrounding electrodes as well as from the central electrode were analyzed together. In this case, the best clustering solution, with the highest median silhouette value, yielded five clusters (Fig. 4c and d – bottom panel). These putative individual cells had no refractory period violations.

The median silhouette value increased from 0.5 to 0.9, when the signals of the six surrounding electrodes were included, suggesting a better grouping of the data (Fig. 4e).

This improvement is achieved, as the added spatial information increases the separability of the waveforms produced by different neurons within the PCA feature space.

3.4. Physiological characterization of retinal ganglion cells

The ability to record from high-density blocks allows for recording from a large proportion of the densely packed RGCs of the mouse retina. Indeed, with the MEA system used here, there is more than one electrode available per RGC as the density of electrodes, 3161 electrodes/mm², is greater than the density of RGCs in the mouse, which amounts to approximately 2700 cells/mm² (Jeon et al., 1998). As described above, the activity of single neurons is picked up on multiple electrodes, enabling us to regularly identify on average 42 ± 7 neurons simultaneously during light stimulation in an area of 0.025 mm² (Fig. 5a). An example of the population of cells, from which we recorded, contained some of the expected cell types. This included RGCs that respond to increases in light intensity (ON RGCs, Fig. 5b–d), decreases in light intensity (OFF RGCs, Fig. 5e and f) or to both, increases and decreases in light intensity (ON–OFF RGCs, Fig. 5g and h). In addition RGCs that were sensitive to a precise direction of motion of the light stimulus were characterized (Figs. 5g, h and Fig. 6).

In this specific case, RGCs were characterized based on their preference to an increase or a decrease of light intensity and to the eventual preference toward a defined direction of motion of a moving bar (see [Light Stimulation in Supplementary Material](#)).

Thus, the high density of electrodes is useful not only for spike sorting, but increases the possibility to find a RGC of interest in the ganglion cell layer, where these neurons are densely packed and their extracellular action potentials mix on single electrodes. In particular, Fig. 5a demonstrates that cells with highly overlapping electrical footprints, the receptive fields of which are overlapping

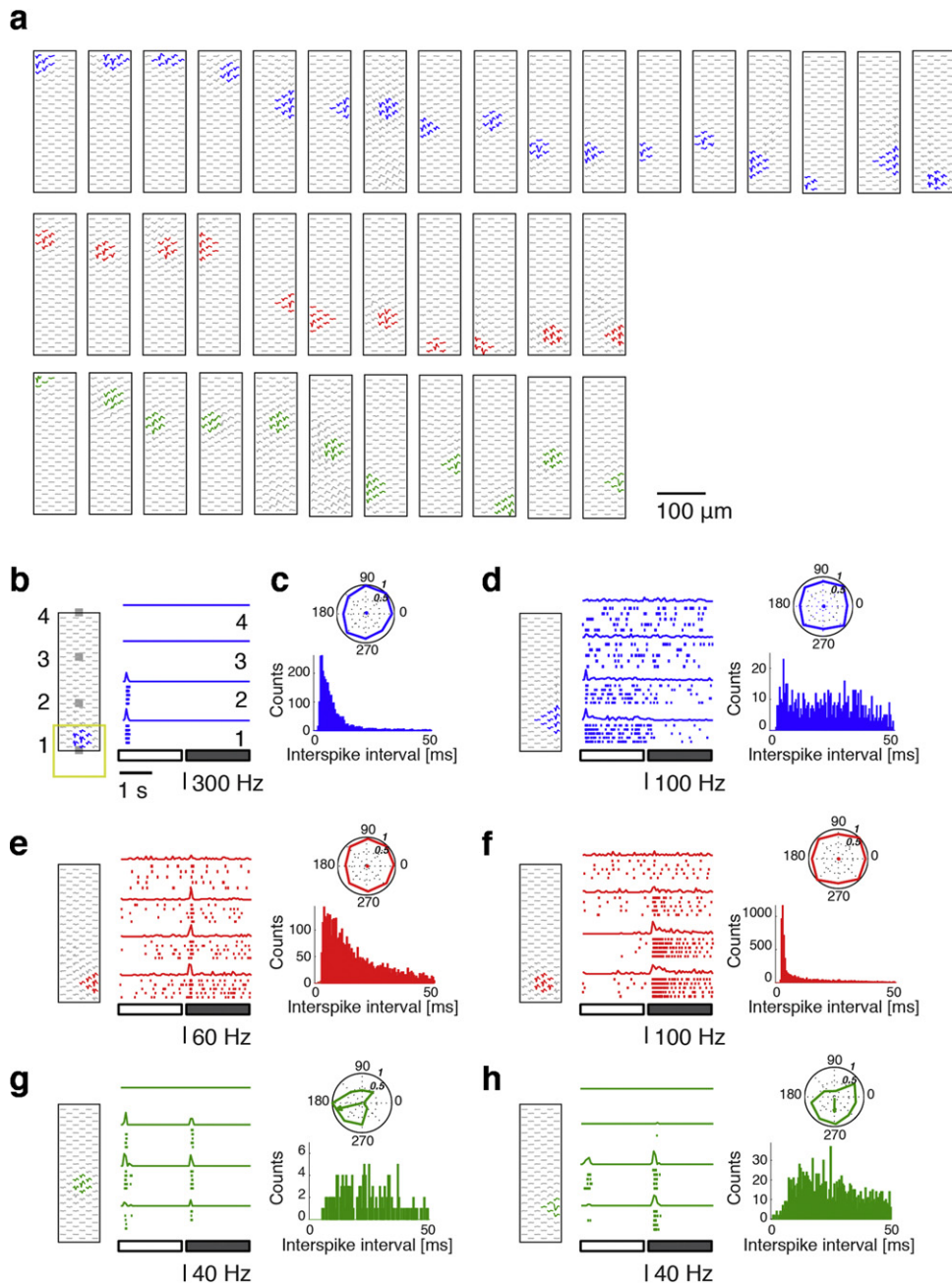


Fig. 5. Physiological responses of mouse retinal ganglion cells. (a) Overlapping footprints of 39 different RGCs on a high-density electrode block (3161 electrodes/mm²). Blue = ON RGCs, red = OFF RGCs, green = ON–OFF RGCs. This shows the possibility of separating RGCs despite physical overlapping of the neuronal extracellular action potential fields. (b) Left panel: mouse RGC footprint (blue) and light stimulus (yellow square, see [Marching Square in Supplementary Material](#)). The four small gray squares indicate four locations, spaced 100 μ m apart, where the light stimulus was sequentially centered. Right panel: four raster plots showing the RGC response to light stimulation, each dot represents a single action potential. There are four different raster plots, because the light stimulus was centered at four different locations. In each raster plot the response to five repetitions of the same stimulus is shown. The firing rate of the RGC is computed by averaging these five responses (long horizontal line at the top of each raster plot). The white bar at the bottom of the raster plots represents “light on” and indicates an increase in light intensity of the stimulus. The gray bar at the bottom of the raster plots represents “light off” and indicates a decrease in light intensity of the stimulus. This cell is classified as ON-RGC, because it responds exclusively to increases in light intensity. According to the response to this light stimulation, it is possible to classify RGCs as: ON (if they respond to an increase of light intensity of the stimulus, b–d); OFF (if they respond to a decrease of light intensity of the stimulus, e–f); ON–OFF (if they respond to both, an increase and a decrease of light intensity of the stimulus, g–h). (c) Top panel: polar plot showing the responses of the RGC in (b) to motion of a bar in 8 directions at 45° radial intervals (see [Moving Bar in Supplementary Material](#)). The response is quantified by counting the number of action potentials that were fired by the RGC in response to the bar moving along the different directions. The tuning curve is normalized to the largest response. The arrow indicates the vector sum response corresponding to the preferred direction. The length of the arrow indicates the extent of direction-selectivity (the arrow is visible in g–h, because these two RGCs are direction-selective, whereas RGCs in b–f are not direction-selective and, therefore, the arrow is too short to be visualized). Bottom panel: distribution of time intervals between consecutive spikes (inter-spike interval distribution). (d–h) Same as in (b and c) and showing the characterization of five neighboring RGCs. (For interpretation of the references to color in this figure legend, the reader is referred to the web version of the article.)

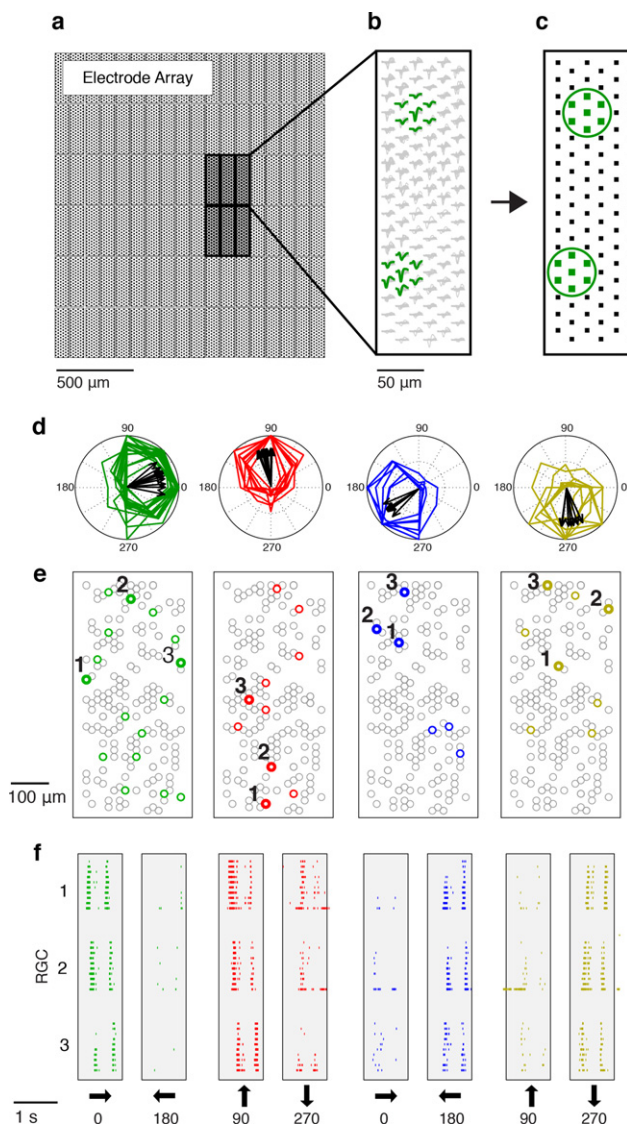


Fig. 6. Strategy to select and record from a defined population of retinal ganglion cells. (a) A region of interest within the piece of retina is stimulated with light and sequentially recorded from using high-density electrode blocks (3161 electrodes per mm²). (b) Action potentials from densely packed RGCs are sorted and classified, based on their physiological responses to light stimulation (see [Light Stimulation in Supplementary Material and Fig. 5](#)). (c) A defined subset of electrodes is selected at the location of a RGC of interest; these electrodes are selected so as to obtain the highest signals for each targeted RGC. (d) Polar plots of four types of selected ON–OFF direction-selective RGCs (Briggman et al., 2011). Each tuning curve has been normalized to the largest response. The black arrow indicates the direction, in which the neurons respond most vigorously, the “preferred direction.” (e) Spatial location of ON–OFF direction-selective RGCs (green, red, blue, yellow circles) across an area of six adjacent high-density electrode blocks. Gray circles indicate the remaining detected RGCs that were not classified as ON–OFF RGCs. (f) Raster plots (10 repetitions, see [Moving Bar in Supplementary Material](#)) from four types of ON–OFF direction-selective RGCs. The gray-shaded rectangles indicate the time, during which the bar was moving across the retina. The black arrow indicates the direction of motion. (For interpretation of the references to color in this figure legend, the reader is referred to the web version of the article.)

to even a much larger extent (see [Fig. 3d](#)), can be detected and assigned.

3.5. Selecting a defined population of retinal ganglion cells for extracellular recordings

Here we demonstrate the ability to target a specific population of RGCs by taking advantage of the high-density packing of the

electrodes and high signal-to-noise ratio of the recordings as well as the rapid dynamic configurability of the MEA system.

To show the effectiveness of this procedure we chose to target ON–OFF direction-selective ganglion cells (Barlow et al., 1964; Weng et al., 2005). The main reason for choosing direction-selective cells is that they have a very characteristic response to light stimulation, making them easily identifiable ([Fig. 5g and h](#)). In fact, ON–OFF direction-selective RGCs respond most vigorously, with a transient burst of action potentials, to light stimuli moving along a preferred direction. Furthermore, they have almost no response to light stimuli moving along the null direction (opposite $\sim 180^\circ$ to the preferred direction). There are four types of ON–OFF direction-selective RGCs (Barlow et al., 1964; Briggman et al., 2011).

In order to target direction-selective RGCs, we first screened a region of interest by recording the activity of all RGCs from a set of highest-density electrode blocks. We scanned six adjacent regions of the ganglion cell layer, spanning an area of 0.15 mm² ([Fig. 6a](#)). During the recording from each electrode configuration block, a search stimulus consisting of a bar that moved in 8 different directions was presented (see [Moving Bar in Supplementary Material](#)).

In the second step, online spike sorting during the experiment was performed (Jackel et al., 2012) (see [Spike Sorting in Supplementary Material](#)), and the sorted neurons were physiologically classified according to their response to light stimulation ([Fig. 6b](#)). During the online analysis, each isolated RGC was tested for its preference for ON vs. OFF stimuli and for its preference for a direction of motion.

Finally, for every RGC of interest, between 5 and 7 electrodes that feature the largest-amplitude signals have been assigned to record from the respective RGCs during the rest of the experiment ([Fig. 6c](#)).

Out of the 212 cells recorded, we found 40 ON–OFF direction selective RGCs and noted their locations ([Fig. 6d and e](#)). Finally, we targeted electrodes to a subset of ON–OFF direction-selective RGCs with the same preferred direction ([Fig. 6e and f](#)).

This allows us to simultaneously record from a group of identified cells of a defined type and to characterize not only the individual but also their collective responses to the applied light stimuli. Within 90 minutes, we were able to probe a 0.15 mm² area of the retina and to select a physiologically defined population of cells that could then be targeted with specific light stimulation for the next ~ 7 hours.

3.6. Recording from genetically identified retinal ganglion cells

Optogenetics is a powerful tool for investigating neuronal cell types and circuits (Yizhar et al., 2011) and an additional way to identify certain cell types. To demonstrate that optogenetics can be used in combination with our CMOS-based MEA we expressed a bi-stable channelrhodopsin (bi-ChR2) (Berndt et al., 2009) in genetically identified RGCs (see [Section 2](#)). bi-ChR2-induced action potentials ([Fig. 7a](#)) were isolated from photoreceptor-triggered action potentials by blocking glutamatergic synaptic transmission (ABP, CPP, NBQX, see [Section 2](#)). In the presence of these blockers, only RGCs expressing ChR2 and the intrinsically photosensitive RGCs (ipRGCs) produced light-induced action potentials. ChR2-induced neuronal firing features shorter response latency than the latency of ipRGCs ([Fig. 7b](#)).

4. Discussion

Retinal circuits encode the visual scene in parallel channels, where each RGC type conveys a different representation (Farrow and Masland, 2011; Roska and Werblin, 2001). The relative timing

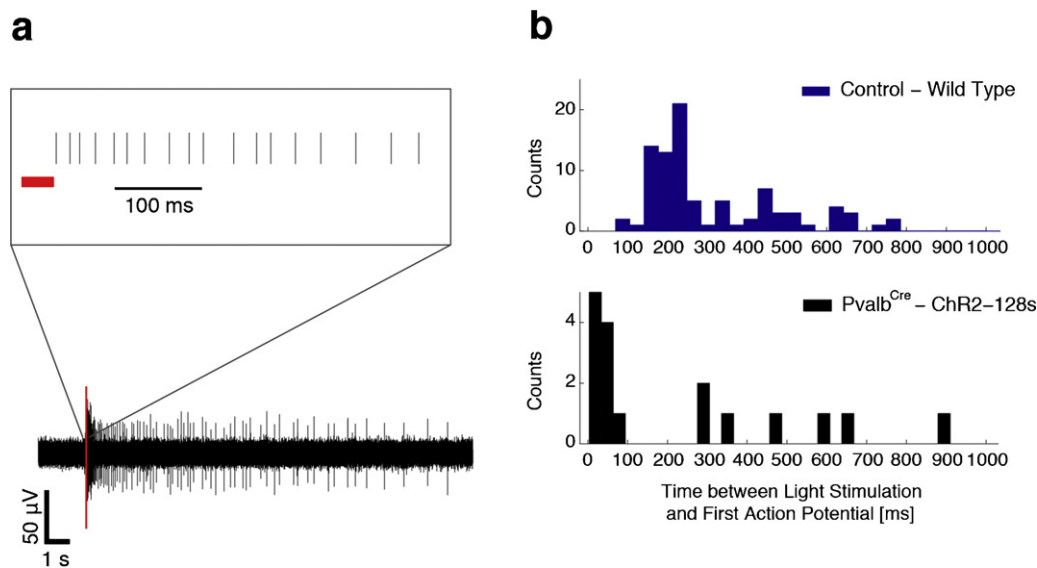


Fig. 7. Recording genetically identified RGCs by optogenetic methods. (a) Trace showing action potentials from a *Pvalb* RGC expressing ChR2-128s light-sensitive cation channels. The inset shows 500 ms raster plot after a 40 ms light pulse. The red line indicates the light pulse. (b) Top panel: distribution of times between light stimulation offset and the first action potential in experiments with wild type retinæ (control). In this experiments there are not RGCs expressing ChR2. Bottom panel: distribution of times between light stimulation offset and the first action potential in experiments with *Pvalb* RGCs expressing ChR2. Note the presence of the early peak in the histogram of the *Pvalb*^{Cre}-ChR2-128S retinæ (b) and the lack of short latencies in the control experiment with wild type retinæ (a). Photoreceptor-mediated light response was blocked in all experiments by using synaptic blockers (see Section 2). (For interpretation of the references to color in this figure legend, the reader is referred to the web version of the article.)

of activity among RGCs has been shown to be relevant for visual encoding (Ackert et al., 2006; Gollisch and Meister, 2008; Schwartz et al., 2007). Furthermore, the study of physiologically identified ganglion cells types demonstrates that time correlations convey significant information about the visual stimulus (Ackert et al., 2006; Pillow et al., 2008). The ability to target specific populations of RGCs is, therefore, a prerequisite for the design of experiments, aimed at understanding the population code of individual as well as combinations of visual channels.

In order to select defined populations of RGCs, we found the following process to be efficient: scanning the MEA for activity characteristic of the RGCs of interest, performing online spike sorting, and, finally, selecting a configuration of electrodes that could most effectively be used to stimulate and record from chosen RGCs.

Elimination of the light artifact in the recorded signal greatly facilitated the quality of the data recorded from the RGCs. This is a pivotal finding, as the activity of the RGCs must be triggered by a light stimulus, while light-induced responses are simultaneously recorded by the MEA. Any artifact that would occur during recording would obscure or add noise to the extracellular action potentials. As a consequence, spike sorting could be rendered unnecessarily challenging with the possibility to completely miss action potentials. As described, the proper focusing of the light stimulus on the electrode array ensures that no artifacts occur.

In order to select a defined population of neurons, a fast and efficient online spike sorting technique is essential to classify the different cell types online during the experiment. To that end, we are currently also exploring spike sorting methods based on ICA (Brown et al., 2001; Harris et al., 2000) and template matching (Franke et al., 2010; Segev et al., 2004), which can optimally utilize the information provided by larger numbers of electrodes per neuron and concurrently reduce signal redundancy.

Furthermore, we here demonstrate that a basic and, admittedly, simple spike sorting algorithm (K-means – and use of silhouette coefficients) can then be used afterwards offline to separate action potentials from highly overlapping neurons of the retinal ensemble due to the fact that (i) the electrode with highest signal-to-noise

ratio can be selected for every neuron for event detection, and (ii) the unique spatial distribution of the action potentials of every neuron, in the highly overlapping retinal ensemble, can be characterized.

This combination of spike sorting methods at different stages has proven to be very successful.

The quality of the spike sorting, finally, is critically depending on the signal quality (signal-to-noise ratio) and the electrode spacing, i.e., the average number of electrodes available to record from a neuron, with every mouse RGC being detectable here, on average, in an area of $65 \mu\text{m} \times 65 \mu\text{m}$. This MEA features an inter-electrode spacing of $18 \mu\text{m}$, and noise levels of $\sim 7 \mu\text{V}_{\text{rms}}$. Besides the possibility to potentially record from every neuron (electrode density larger than neuronal density), the overall surface that is covered with electrodes is an important parameter, as it is desirable to monitor many neurons of the same distinct type to investigate colony or population responses. (For more details and a comparison between different MEA devices, please see also Fig. S2 in the Supplementary Material.)

Relative to devices previously used for retinal studies, Zeck et al. recently published a study on axonal action potentials in the rabbit retina using a CMOS-based MEA (Zeck et al., 2011). The device featured 16,384 sensor transistors at spatial resolution of $7.4 \mu\text{m}$ ($16,384$ electrodes/ mm^2) on an area of $1 \text{mm} \times 1 \text{mm}$ and a sampling rate of 6 kHz (Lambacher et al., 2011). The work by Zeck et al. demonstrates the importance of using a MEA that features a high density of electrodes for studying the propagation speed of action potentials along axons of different RGCs types. The MEA used by Zeck et al. features noise levels from 50 to $250 \mu\text{V}_{\text{rms}}$, which allows the isolation of action potentials with amplitudes as low as $200 \mu\text{V}$ (Lambacher et al., 2011). Such noise levels render the characterization of small RGCs with low-amplitude action potentials difficult.

The CMOS-based MEA by Berdondini et al. has 4096 on an area of $2.67 \text{mm} \times 2.67 \text{mm}$, a sampling rate of 7.8 kHz and noise levels of $\sim 11 \mu\text{V}_{\text{rms}}$ (Berdondini et al., 2009). The use of light stimulation with this device has not yet been reported. The density of mouse RGCs (2700 cells/ mm^2 , Jeon et al., 1998) is about 4.7 times

higher than the MEA electrode density (567 electrodes/mm²). As a consequence, finding and targeting a defined population of mouse RGCs as well as to accurately sort their action potentials would be difficult.

The MEA system designed by Litke et al. was successfully used to record the activity of defined populations of RGCs and to study photoreceptor connectivity in the periphery of the macaque monkey retina (Field et al., 2010; Litke et al., 2004; Pillow et al., 2008). The circuitless device used by Litke et al. features 512 electrodes at a spatial resolution of 60 μm (321 electrodes/mm²) on an area of 1.7 mm² and a sampling rate of 20 kHz. In the context of the mouse retina, a spatial resolution of 60 μm decreases the number of electrodes available per neuron, which decreases the performance of the spike sorting and, therefore, reduces the possibilities to allocate the densely packed RGCs.

The circuitless MEA systems used by Segev et al. features 30 electrodes at a spatial resolution of 30 μm (1111 electrodes/mm²) over an area of 0.12 mm × 0.15 mm (Segev et al., 2004). Although this MEA device features a comparably high electrode density and low noise levels, it is limited by the low overall number of electrodes that allow the study of only small retina regions.

In summary, the developed methodology to find, locate, and to selectively record from or target a distinct type of neuronal cell that can be identified, either according to the respective signaling behavior upon specific stimuli, or by applying optogenetic methods, constitutes an important neuroscientific tool. This tool can be used to investigate population-specific signaling in different types of preparations, including retinæ, brain slices, or dissociated neuronal cultures. We demonstrated that distinct neuronal populations (e.g., all 4 different types of ON–OFF direction-selective cells) can be assigned and discerned in the retina. Furthermore, we demonstrated our technique in the mouse, where genetic tools are available and genetically identified retinal ganglion cell types have been identified (Huberman et al., 2009; Kim et al., 2008; Munch et al., 2009). In future studies, this developed cell identification-and-targeting system will be used to target defined physiological types of RGCs in an effort to decode elements of the retinal code. Recording of synchronous action potentials from defined cell types will lead to a more complete understanding of how the retina as a whole encodes a visual scene and what the code is that the brain then uses to interpret the retinal data (Pillow et al., 2008).

Acknowledgements

This work was financially supported by the FP7 of the European Community through the ERC Advanced Grant 267351 “NeuroCMOS”. Michele Fiscella acknowledges individual support through a Swiss SystemsX interdisciplinary PhD grant 2009.031. Karl Farrow acknowledges individual support through Marie Curie and EMBO long-term fellowships. We acknowledge Miguel H. Teixeira for imaging of mouse retinal ganglion cells.

Appendix A. Supplementary data

Supplementary data associated with this article can be found, in the online version, at <http://dx.doi.org/10.1016/j.jneumeth.2012.08.017>.

References

- Ackert JM, Wu SH, Lee JC, Abrams J, Hu EH, Perlman I, et al. Light-induced changes in spike synchronization between coupled ON direction selective ganglion cells in the mammalian retina. *J Neurosci* 2006;26:4206–15.
- Anishchenko A, Greschner M, Elstrott J, Sher A, Litke AM, Feller MB, et al. Receptive field mosaics of retinal ganglion cells are established without visual experience. *J Neurophysiol* 2010;103:1856–64.
- Barlow HB, Hill RM, Levick WR. Retinal ganglion cells responding selectively to direction and speed of image motion in the rabbit. *J Physiol* 1964;173:377–407.
- Berdondini L, Imfeld K, Maccione A, Tedesco M, Neukom S, Koudelka-Hep M, et al. Active pixel sensor array for high spatio-temporal resolution electrophysiological recordings from single cell to large scale neuronal networks. *Lab Chip* 2009;9:2644–51.
- Berndt A, Yizhar O, Gunaydin LA, Hegemann P, Deisseroth K. Bi-stable neural state switches. *Nat Neurosci* 2009;12:229–34.
- Berson DM, Dunn FA, Takao M. Phototransduction by retinal ganglion cells that set the circadian clock. *Science* 2002;295:1070–3.
- Bi A, Cui J, Ma YP, Olshevskaya E, Pu M, Dizhoor AM, et al. Ectopic expression of a microbial-type rhodopsin restores visual responses in mice with photoreceptor degeneration. *Neuron* 2006;50:23–33.
- Boiko T, Rasband MN, Levinson SR, Caldwell JH, Mandel G, Trimmer JS, et al. Compact myelin dictates the differential targeting of two sodium channel isoforms in the same axon. *Neuron* 2001;30:91–104.
- Briggman KL, Helmstaedter M, Denk W. Wiring specificity in the direction-selectivity circuit of the retina. *Nature* 2011;471:183–8.
- Brown GD, Yamada S, Sejnowski TJ. Independent component analysis at the neural cocktail party. *Trends Neurosci* 2001;24:54–63.
- Brown SP, He S, Masland RH. Receptive field microstructure and dendritic geometry of retinal ganglion cells. *Neuron* 2000;27:371–83.
- Chichilnisky EJ. A simple white noise analysis of neuronal light responses. *Network* 2001;12:199–213.
- Darmont A. Spectral response of silicon image sensors; 2009. www.aphesa.com.
- Ding L, Ye JD, Liu Y, Wong JI, Fung SHY, Cen ZH, et al. Optical transmission and photoluminescence of silicon nitride thin films implanted with Si ions. *Electrochim Solid State Lett* 2009;12:H38–40.
- Duda RO, Hart PE, Stork DG. Duda RO, Hart PE, Stork DG, editors. Pattern classification and scene analysis. Pattern classification. 2nd ed. New York; Chichester: Wiley; 2001.
- Elstrott J, Anishchenko A, Greschner M, Sher A, Litke AM, Chichilnisky EJ, et al. Direction selectivity in the retina is established independent of visual experience and cholinergic retinal waves. *Neuron* 2008;58:499–506.
- Eversmann B, Jenkner M, Hofmann F, Paulus C, Brederlow R, Holzapfl B, et al. A 128 × 128 CMOS biosensor array for extracellular recording of neural activity. *IEEE J Solid-State Circuits* 2003;38:2306–17.
- Farrow K, Masland RH. Physiological clustering of visual channels in the mouse retina. *J Neurophysiol* 2011;105:1516–30.
- Field GD, Gauthier JL, Sher A, Greschner M, Machado TA, Jepsen LH, et al. Functional connectivity in the retina at the resolution of photoreceptors. *Nature* 2010;467:673–7.
- Franke F, Natora M, Boucsein C, Munk MH, Obermayer K. An online spike detection and spike classification algorithm capable of instantaneous resolution of overlapping spikes. *J Comput Neurosci* 2010;29:127–48.
- Frey U, Egert U, Heer F, Hafizovic S, Hierlemann A. Microelectronic system for high-resolution mapping of extracellular electric fields applied to brain slices. *Biosens Bioelectron* 2009;24:2191–8.
- Frey U, Sedivy J, Heer F, Pedron R, Ballini M, Mueller J, et al. Switch-matrix-based high-density microelectrode array in CMOS technology. *IEEE J Solid-State Circuits* 2010;45.
- Gold C, Henze DA, Koch C, Buzsaki G. On the origin of the extracellular action potential waveform: a modeling study. *J Neurophysiol* 2006;95:3113–28.
- Gollisch T, Meister M. Rapid neural coding in the retina with relative spike latencies. *Science* 2008;319:1108–11.
- Gross GW, Rhoades BK, Azzazy HM, Wu MC. The use of neuronal networks on multi-electrode arrays as biosensors. *Biosens Bioelectron* 1995;10:553–67.
- Harris KD, Henze DA, Csicsvari J, Hirase H, Buzsaki G. Accuracy of tetrad spike separation as determined by simultaneous intracellular and extracellular measurements. *J Neurophysiol* 2000;84:401–14.
- Huberman AD, Wei W, Elstrott J, Stafford BK, Feller MB, Barres BA. Genetic identification of an ON–OFF direction-selective retinal ganglion cell subtype reveals a layer-specific subcortical map of posterior motion. *Neuron* 2009;62:327–34.
- Jackel D, Frey U, Fiscella M, Franke F, Hierlemann A. Applicability of independent component analysis on high-density microelectrode array recordings. *J Neurophysiol* 2012;108:334–48.
- Jeon CJ, Strettoi E, Masland RH. The major cell populations of the mouse retina. *J Neurosci* 1998;18:8936–46.
- Jimbo Y, Robinson HP, Kawana A. Strengthening of synchronized activity by tetanic stimulation in cortical cultures: application of planar electrode arrays. *IEEE Trans Biomed Eng* 1998;45:1297–304.
- Jones IL, Fiscella M, Frey U, Jackel D, Muller J, Rosic B, et al. Recording of neural activity of mouse retinal ganglion cells by means of an integrated high-density microelectrode array. In: The 16th international conference on solid-state sensors, actuators and microsystems, transducers; 2011. p. 186–9.
- Kim IJ, Zhang Y, Yamagata M, Meister M, Sanes JR. Molecular identification of a retinal cell type that responds to upward motion. *Nature* 2008;452:478–82.
- Lagali PS, Balya D, Awatramani GB, Munch TA, Kim DS, Busskamp V, et al. Light-activated channels targeted to ON bipolar cells restore visual function in retinal degeneration. *Nat Neurosci* 2008;11:667–75.
- Lambacher A, Jenkner M, Merz M, Eversmann B, Kaul RA, Hofmann F, et al. Electrical imaging of neuronal activity by multi-transistor-array (MTA) recording at 7.8 μm. *Resolut Appl Phys A: Mater Sci Proc* 2004;79:1607–11.
- Lambacher A, Vitzthum V, Zeitler R, Eickenscheidt M, Eversmann B, Thewes R, et al. Identifying firing mammalian neurons in networks with high-resolution multi-transistor array (MTA). *Appl Phys A* 2011;102:1–11.

- Lewicki MS. A review of methods for spike sorting: the detection and classification of neural action potentials. *Network* 1998;9:R53–78.
- Litke AM, Bezaif N, Chichilnisky EJ, Cunningham W, Dabrowski W, Grillo AA, et al. What does the eye tell the brain? Development of a system for the large-scale recording of retinal output activity. *IEEE Trans Nucl Sci* 2004;51:1434–40.
- Masland RH. The fundamental plan of the retina. *Nat Neurosci* 2001;4:877–86.
- Meister M, Pine J, Baylor DA. Multi-neuronal signals from the retina: acquisition and analysis. *J Neurosci Methods* 1994;51:95–106.
- Munch TA, da Silveira RA, Siegert S, Viney TJ, Awatramani GB, Roska B. Approach sensitivity in the retina processed by a multifunctional neural circuit. *Nat Neurosci* 2009;12:1308–16.
- Oyster CW, Takahashi ES, Fry KR, Lam DM. Ganglion cell density in albino and pigmented rabbit retinas labeled with a ganglion cell-specific monoclonal antibody. *Brain Res* 1987;425:25–33.
- Perry VH, Cowey A. The ganglion cell and cone distributions in the monkey's retina: implications for central magnification factors. *Vis Res* 1985;25:1795–810.
- Pillow JW, Shlens J, Paninski L, Sher A, Litke AM, Chichilnisky EJ, et al. Spatio-temporal correlations and visual signalling in a complete neuronal population. *Nature* 2008;454:995–9.
- Pine J. Recording action potentials from cultured neurons with extracellular micro-circuit electrodes. *J Neurosci Methods* 1980;2:19–31.
- Puchalla JL, Schneidman E, Harris RA, Berry MJ. Redundancy in the population code of the retina. *Neuron* 2005;46:493–504.
- Roska B, Werblin FS. Vertical interactions across ten parallel, stacked representations in the mammalian retina. *Nature* 2001;410:583–7.
- Rousseeuw JP. Silhouettes: a graphical aid to the interpretation and validation of cluster analysis. *J Comput Appl Math* 1987;20:56–65.
- Rutten WL. Selective electrical interfaces with the nervous system. *Annu Rev Biomed Eng* 2002;4:407–52.
- Schwartz G, Taylor S, Fisher C, Harris R, Berry 2nd MJ. Synchronized firing among retinal ganglion cells signals motion reversal. *Neuron* 2007;55:958–69.
- Segev R, Goodhouse J, Puchalla J, Berry MJ. Recording spikes from a large fraction of the ganglion cells in a retinal patch. *Nat Neurosci* 2004;7:1154–61.
- Sekirnjak C, Hottowy P, Sher A, Dabrowski W, Litke AM, Chichilnisky EJ. High-resolution electrical stimulation of primate retina for epiretinal implant design. *J Neurosci* 2008;28:4446–56.
- Stett A, Eger U, Guenther E, Hofmann F, Meyer T, Nisch W, et al. Biological application of microelectrode arrays in drug discovery and basic research. *Anal Bioanal Chem* 2003;377:486–95.
- Sun W, Li N, He S. Large-scale morphological survey of mouse retinal ganglion cells. *J Comp Neurol* 2002;451:115–26.
- Trong PK, Rieke F. Origin of correlated activity between parasol retinal ganglion cells. *Nat Neurosci* 2008;11:1343–51.
- Wassle H. Parallel processing in the mammalian retina. *Nat Rev Neurosci* 2004;5:747–57.
- Weng S, Sun W, He S. Identification of ON–OFF direction-selective ganglion cells in the mouse retina. *J Physiol* 2005;562:915–23.
- Wong KY, Dunn FA, Graham DM, Berson DM. Synaptic influences on rat ganglion-cell photoreceptors. *J Physiol* 2007;582:279–96.
- Yizhar O, Fenno LE, Davidson TJ, Mogri M, Deisseroth K. Optogenetics in neural systems. *Neuron* 2011;71:9–34.
- Yonehara K, Balint K, Noda M, Nagel G, Bamberg E, Roska B. Spatially asymmetric reorganization of inhibition establishes a motion-sensitive circuit. *Nature* 2011;469:407–10.
- Zeck G, Lambacher A, Fromherz P. Axonal transmission in the retina introduces a small dispersion of relative timing in the ganglion cell population response. *PLoS ONE* 2011;6:e20810.